Nonlinear gyrokinetic simulations of the I-mode high confinement regime and comparisons with experimenta)

Nonlinear gyrokinetic simulations of the I-mode high confinement regime and comparisons with experiment

A. E. White', N. T. Howard, A. J. Creely, M. A. Chilenski, M. Greenwald, A. E. Hubbard, J. W. Hughes, E. Marmar, J. E. Rice, J. M. Sierchio, C. Sung, J. R. Walk, D. G. Whyte, D. R. Mikkelsen, E. M. Edlund, C. Kung, C. Holland, J. Candy, C. C. Petty, M. L. Reinke, and C. Theiler

Citation: Physics of Plasmas **22**, 056109 (2015); doi: 10.1063/1.4921150

View online: http://dx.doi.org/10.1063/1.4921150

View Table of Contents: http://aip.scitation.org/toc/php/22/5

Published by the American Institute of Physics

Nonlinear gyrokinetic simulations of the I-mode high confinement regime and comparisons with experiment[a)]

A. E. White,[1,b),c)] N. T. Howard,[1] A. J. Creely,[1] M. A. Chilenski,[1] M. Greenwald,[1] A. E. Hubbard,[1] J. W. Hughes,[1] E. Marmar,[1] J. E. Rice,[1] J. M. Sierchio,[1] C. Sung,[1] J. R. Walk,[1] D. G. Whyte,[1] D. R. Mikkelsen,[2] E. M. Edlund,[2] C. Kung,[2] C. Holland,[3] J. Candy,[4] C. C. Petty,[4] M. L. Reinke,[5] and C. Theiler[6]

[1]*MIT Plasma Science and Fusion Center, Cambridge, Massachusetts 02139, USA*
[2]*Princeton Plasma Physics Laboratory, Princeton, New Jersey 08540, USA*
[3]*University of California, San Diego (UCSD) San Diego, California 92093, USA*
[4]*General Atomics, P.O. Box 85608, San Diego, California 92186, USA*
[5]*York University, Heslington, York YO10 5DD, United Kingdom*
[6]*Centre de Recherches en Physique des Plasmas, Ecole Polytechnique Federale de Lausanne, Lausanne 1015, Switzerland*

(Received 22 December 2014; accepted 13 April 2015; published online 14 May 2015)

For the first time, nonlinear gyrokinetic simulations of I-mode plasmas are performed and compared with experiment. I-mode is a high confinement regime, featuring energy confinement similar to H-mode, but without enhanced particle and impurity particle confinement [D. G. Whyte *et al.*, Nucl. Fusion **50**, 105005 (2010)]. As a consequence of the separation between heat and particle transport, I-mode exhibits several favorable characteristics compared to H-mode. The nonlinear gyrokinetic code GYRO [J. Candy and R. E. Waltz, J Comput. Phys. **186**, 545 (2003)] is used to explore the effects of $E \times B$ shear and profile stiffness in I-mode and compare with L-mode. The nonlinear GYRO simulations show that I-mode core ion temperature and electron temperature profiles are more stiff than L-mode core plasmas. Scans of the input $E \times B$ shear in GYRO simulations show that $E \times B$ shearing of turbulence is a stronger effect in the core of I-mode than L-mode. The nonlinear simulations match the observed reductions in long wavelength density fluctuation levels across the L-I transition but underestimate the reduction of long wavelength electron temperature fluctuation levels. The comparisons between experiment and gyrokinetic simulations for I-mode suggest that increased $E \times B$ shearing of turbulence combined with increased profile stiffness are responsible for the reductions in core turbulence observed in the experiment, and that I-mode resembles H-mode plasmas more than L-mode plasmas with regards to marginal stability and temperature profile stiffness. © *2015 AIP Publishing LLC*.
[http://dx.doi.org/10.1063/1.4921150]

I. INTRODUCTION

I-mode is a high confinement regime, featuring energy confinement similar to H-mode, but without enhanced particle and impurity particle confinement.[1] As a consequence of the separation between heat and particle transport, I-mode exhibits several favorable characteristics compared to H-mode. Because there is only an edge temperature pedestal and no edge density pedestal, I-mode pedestals are stable to ELMs (Edge Localized Modes)[2] and are experimentally observed to be generally ELM-free. Even without ELMs, I-modes do not have core impurity accumulation, resulting in reduced impurity radiation with a high-Z metal wall. I-mode plasmas have been run on Alcator C-Mod,[3,4] ASDEX Upgrade,[5] and DIII-D.[6] Cross-machine comparisons of global scalings and pedestal characteristics in I-mode have been recently presented.[6] The general features of the I-mode regime have been described in the previous work,[2–4,7] with emphasis on the pedestal and edge regions. Observations of reduced core turbulence and transport in I-mode have also been reported on previously.[8]

I-mode characteristics make it a favorable regime for operation on ITER and other future devices, so it is important to determine if I-mode core transport can be well-described using existing gyrokinetic and gyrofluid transport models. These transport models, such as the Multi Mode,[9] IFS/PPPL,[10] GLF23 models,[11] and TGLF models,[12] are currently used to understand and predict H-mode performance in ITER.[13] These transport models include the characteristics known as stiffness and critical gradient, which are predicted by nonlinear gyrokinetic theory,[10,14,15] and which can be related to underlying turbulent modes which are stable below the critical gradient threshold and unstable above it.[16] Experimental evidence for profile stiffness and critical gradients is also found in several tokamaks.[17–23]

As a consequence of stiff transport in the plasma core, the edge temperature provides the key boundary condition dictating overall plasma performance.[10,14,24] This means that in very stiff core plasmas, like many H-modes, small decreases/increases in local temperature gradients can lead

[a)]Paper NI1 1, Bull. Am. Phys. Soc. **59**, 191 (2014).
[b)]Invited Speaker; 2014 Recipient of the Catherine E. Weimer Award for Women in Plasma Science.
[c)]whitea@mit.edu

to large decreases/increases in local diffusivity. The changes can start at the edge of the plasma, and the modifications to the profile that are constrained by the flux-gradient response (i.e., the stiffness) will propagate across the profile, with the result being changes in core temperature.[10] Experimentally observed changes in core plasma turbulence and core profiles across L-H[25] and L-I transitions,[8] and more widely observed scaling of core confinement with edge temperature pedestal[26] are consistent with this picture.

In this paper, we present the first nonlinear gyrokinetic simulations of I-mode plasmas. All simulations presented in this paper use the GYRO code[27] to explore the effects of $E \times B$ shear and profile stiffness. We find that ion-scale ($k_\theta \rho_s < 1.4$) local nonlinear simulations can match both ion and electron heat fluxes in I-mode, but the same type of simulations can match only ion heat flux in L-mode, while the electron heat flux is underpredicted. This is consistent with previous L-mode cases from C-Mod that exhibit a robust underprediction of electron heat flux.[28] We note that recent multi-scale simulations including electron scale turbulence ($k_\theta \rho_s < 50$) can resolve the discrepancy in L-modes, while simultaneously matching the ion heat flux,[29] but in this work we only use ion-scale simulations. A series of flux-gradient scans with the nonlinear GYRO simulations show that I-mode core plasmas are more stiff than L-mode core plasmas. These results are significant because they provide new evidence that gyrokinetic and gyrofluid transport models should work well to predict performance in I-mode plasmas. Preliminary TGLF modeling of these I-mode plasmas, not presented here, showed good agreement between predicted profiles and experimental profiles. Scans of the input $E \times B$ shear in GYRO simulations show that $E \times B$ shearing of turbulence is a stronger effect in the core of I-mode than L-mode. The nonlinear simulations match the observed reductions in long wavelength density fluctuation levels across the L-I transition but underestimate the reduction of long wavelength electron temperature fluctuation levels. We conclude that the increased $E \times B$ shearing of turbulence combined with increased profile stiffness are responsible for the observed reductions in core turbulence.

II. EXPERIMENTAL SET-UP

Alcator C-Mod is a high field (2.1 − 8.1 T), compact ($a = 0.22$ m, $R = 0.68$ m) high performance, diverted tokamak, with high-Z metal plasma facing components. Data from a single plasma discharge with an L-I transition (shot 1101209029) are used in this paper for comparisons with nonlinear gyrokinetic simulations, and data from similar plasmas are used to examine trends across L-I transitions. The selected discharge has been described in detail previously.[4,8] The plasma parameters are $\langle n_e \rangle = 2.1 \times 10^{20}$ m^{-3}, $I_p = 1.31$ MA, $B_t = 5.66$ T, $q_{95} = 3.25$. The discharge is operated with the ion ∇B-drift direction pointing away from the active x-point (unfavorable direction), which raises the power threshold for the L-H mode transition. Auxiliary input power from ion cyclotron range of frequency (ICRF) heating is applied, with $P_{ICRF} = 5$ MW.

This particular plasma is selected for comparisons with gyrokinetic codes, because there is very steady density across the L-I transition which allowed for measurements of the evolution of core and edge density fluctuations across the transition with a multi-channel reflectometer. The time history for the discharge is shown in Fig. 1. Across the L-I transition, which begins at $t = 0.875$ s, the core temperature increases as the edge temperature pedestal forms. Edge turbulence measurements with a reflectometer at $r/a = 0.99$ showed reduced broadband turbulent density fluctuations, and the appearance of the Weakly Coherent Mode (WCM), across the L-I transition. Core turbulence measured with a reflectometer at $r/a = 0.55$, showed reduced fluctuations across the L-I transition. The changes in edge and core turbulence persist throughout the I-mode; the changes are not transient. Detailed descriptions of the reduction in core fluctuations are presented in Ref. 8.

The density and electron temperature radial profiles at L-mode and I-mode times of interest were measured with Thomson scattering.[30] The electron temperature profile was also measured with a Grating Polychromator (GPC) electron cyclotron emission (ECE) diagnostic.[31] Ion temperature and toroidal rotation were measured with a high resolution x-ray spectrometer[32] outside of $r/a = 0.35$ in these plasmas, and the radial electric field profile was calculated using TRANSP.[33] Figure 2 shows the fits to the measured density

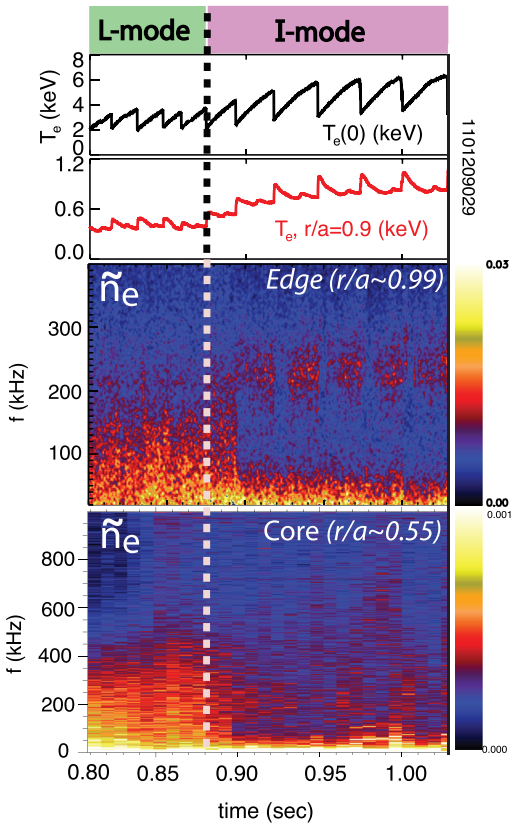

FIG. 1. Time histories from C-Mod plasma with L-I transition. Across the L-I transition beginning at $t = 0.875$ s, the core temperature increases as the edge temperature pedestal forms. Typical edge ($r/a = 0.99$) density fluctuations measured with a reflectometer across the L-I transition showed reduced broadband turbulent density fluctuations, and the appearance of the WCM. Core density fluctuations ($r/a = 0.55$), also measured with a reflectometer, showed reduced fluctuations across the L-I transition.

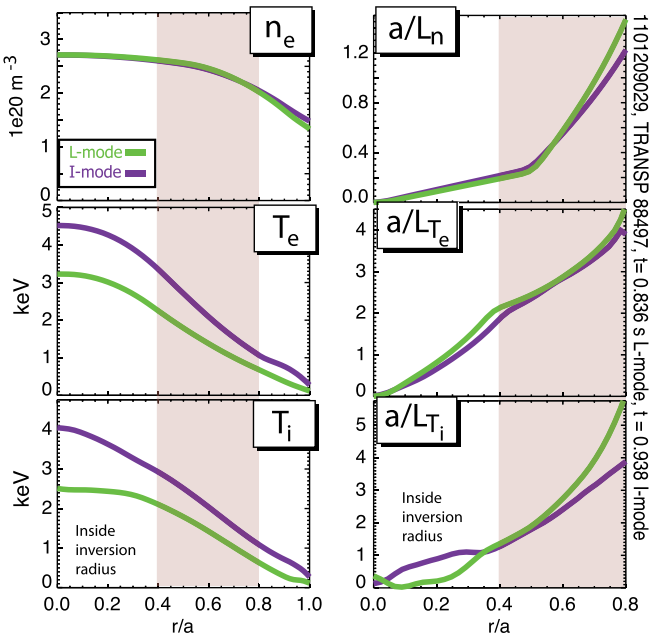

FIG. 2. Profiles from the C-Mod plasma with the L-I transition are shown in Fig. 1. The L-mode time for GYRO analysis is $t = 0.836$ s (profiles shown in green). The I-mode time is t = 0.938 s (purple). Only the radial region outside the sawtooth inversion radius ($r/a > 0.45$) and inside the edge/pedestal ($r/a < 0.8$) is of interest for characterizing the core turbulent-driven transport.

and temperature profiles, averaged over 20 ms, from the C-Mod plasma shown in Fig. 1. The L-mode time point for comparisons with GYRO is a 20 ms average, centered at $t = 0.836$ s (profiles shown in green). The I-mode time point is a 20 ms average, centered at $t = 0.938$ s (purple). Only the radial region outside the sawtooth inversion radius ($r/a > 0.45$) and inside the edge/pedestal ($r/a < 0.8$) is of interest for characterizing the core turbulent-transport. In this region ($0.45 < r/a < 0.8$), the density profile showed little to no change across the L-I transition, while the core electron and ion temperatures increased. The ion temperature gradient scale length tends to decrease outside of $r/a = 0.6$, but electron temperature and density gradient scale lengths changed very little in the range of interest. Based on the fits, estimated errors (1-sigma standard deviations) on the gradient scale lengths are 30% for a/L_{Ti} and 20% for a/L_{Te} and a/L_{ne}. Errors on the $E \times B$ shearing rate are 40%. These experimental errors limit the modifications to GYRO inputs that can be made in order to obtain the so-called "heat flux-matched" GYRO simulations, described later. Power balance analysis with the TRANSP code[33] is performed for this plasma. Estimated errors on the experimental heat fluxes are calculated using error propagation,[34] and this method has been checked to be consistent with brute-force Monte-Carlo methods.[35] The one-sigma standard deviations for the experimental values of ion and electron heat flux give error estimates of 30% for both channels.

III. LOCAL NONLINEAR SIMULATIONS WITH THE GYRO CODE

Local (fixed input profile) nonlinear flux-tube simulations run with the GYRO code[27] are used to model the L-mode and I-mode plasmas. All simulations used in this work are ion-scale simulations, which do not include the electron scale turbulence. Simulations are run at $r/a = 0.6$, and $r/a = 0.8$ for both L-mode and I-mode plasmas, with the radial locations chosen to be near locations of core turbulence measurements in the experiments.[8] The simulations presented are electrostatic and include gyrokinetic ions, drift kinetic electrons, E×B, and rotation effects. The simulations include a single average impurity species (Z = 11; A = 22) based on experimental spectroscopy measurements in similar L-mode and I-modes; so ion dilution is set at 80% in I-mode and 85% in L-mode. The estimated experimental Z_{eff} is taken to be the neoclassical value. In GYRO the dilution and Z_{eff} can be set independently. Both the Z_{eff} and the dilution (average Z) values have experimental uncertainties. Sensitivity scans with the GYRO simulations show that varying dilution and Z_{eff} together (or separately) do not change the heat flux results. Both electron-ion collisions and ion-ion collisions are included. The simulations used 24 toroidal modes and included $k_\theta \rho_s$ up to ≈1.4 in both L-mode and I-mode, so that ion-scale turbulence dynamics are captured. Simulation domain sizes are $L_x = 100\rho_s$, and $L_y = 100\rho_s$, with 464 radial grid points. The input parameters for the four "heat flux-matched" simulations discussed in this paper are given in Table I. These four simulations are carried out using experimental data from the single plasma discharge described in Sec. II, at two different time slices. Many output parameters are normalized. The relevant normalization factors are the sound speed, c_s (m/s), which is $c_s = 2.531 \times 10^5$ (m/s) and 3.112×10^5 (m/s) at $r/a = 0.6$ in L-mode and I-mode, respectively, and $c_s = 1.767 \times 10^5$ (m/s) and $c_s = 2.211 \times 10^5$ (m/s) at $r/a = 0.8$ in L-mode and I-mode, respectively; and the gyroBohm heat flux, Q_{gB} = (MW/m^2), which is $Q_{gB} = 0.121$ (MW/m^2) and 0.336 (MW/m^2) at $r/a = 0.6$ in L-mode and I-mode, respectively, and $Q_{gB} = 0.012$ (MW/m^2) and 0.036 (MW/m^2) at $r/a = 0.8$ in L-mode and I-mode, respectively. In the GYRO code, $Q_{gB} = n_e T_e^{5/2} m_D^{1/2} c^2/(eBa)^2$, where n_e and T_e are electron density and temperature, m_D is deuteron mass, c is the speed of light, a is plasma minor radius, and B is the GYRO defined variable for effective magnetic field strength, B_{unit}.[36] An additional parameter of interest is ν^*, defined as the electron (or ion) collision frequency normalized by the particle's bounce frequency. In L-mode at $r/a = 0.6$, $\nu_i^* = 0.15$ and $\nu_e^* = 0.2$, and at $r/a = 0.8$, $\nu_i^* = 0.6$ and $\nu_e^* = 0.7$. In I-mode at $r/a = 0.6$, $\nu_i^* = 0.08$ and $\nu_e^* = 0.1$, and at $r/a = 0.8$, $\nu_i^* = 0.25$ and $\nu_e^* = 0.3$.

A. Set-up for heat flux-matched simulations

Figure 3 shows the ion heat flux (a) and electron heat flux (b) output from the local GYRO simulation at r/a = 0.6 for L-mode versus simulation time-step. We employ an approach used previously for modeling Neutral Beam heated plasmas at DIII-D,[37] where the simulations are started with E×B shear effects turned off, but with all other experimental values used as input, and then after the linear start-up phase, the $E \times B$ shear is turned on. As shown in Fig. 3 early in the simulation, $t < 50a/c_s$, the heat flux values reach a

TABLE I. This table contains the input parameters used for local GYRO simulations. These are experimental values, except for the values of a/L_{Ti}, which were modified within error bars to match the experimental ion heat flux values. The footnotes list the experimental values for comparison.

Local parameter	L-mode r/a = 0.6	I-mode r/a = 0.6	L-mode r/a = 0.8	I-mode r/a = 0.8
a (m)	0.223	0.223	0.229	2.233
R/a	3.044	3.052	3.029	3.032
T_e (keV)	1.337	2.022	0.652	1.021
n_e (10^{19} m^{-3})	24.43	24.20	19.97	20.02
ρ_s (m)	7.742×10^{-4}	8.294×10^{-4}	3.992×10^{-4}	4.959×10^{-4}
c_s/a (1/s)	1.136×10^{6}	1.393×10^{6}	7.928×10^{5}	9.903×10^{5}
$\rho^* = \rho_s/a$	0.003	0.004	0.002	0.002
ν_{ei} (c_s/a)	0.249	0.111	0.819	0.350
$T_i/T_e = T_z/T_e$	1.036	0.983	0.917	1.024
n_i/n_e	0.850	0.800	0.85	0.80
Z_{eff}	2.5	2.5	2.5	2.5
a/L_{Ti}	2.203[a]	1.849[b]	5.583[c]	3.526[d]
a/L_n	0.606	0.582	1.481	1.252
a/L_{Te}	2.928	2.872	4.239	3.656
Elongation κ	1.312	1.310	1.384	1.387
Triangularity δ	0.126	0.132	0.214	2.227
Shafranov shift Δ	−0.060	−0.085	−0.088	−1.114
Safety factor q	1.238	1.289	1.923	2.008
Shear $\hat{s} = -\frac{r}{q}\frac{dq}{dr}$	1.068	1.086	2.159	2.189
Mach number M (c_s/a)	0.107	0.168	0.056	0.140
$\gamma_{E\times B}$ (c_s/a)	0.042	0.035	0.080	0.083
$\omega 0, Doppler$ (c_s/a)	0.035	0.055	0.018	0.046

[a]22.5% reduction from experimental value $a/L_{Ti} = 2.842$.
[b]26.25% reduction from experimental value $a/L_{Ti} = 2.507$.
[c]10% reduction from experimental value $a/L_{Ti} = 6.204$.
[d]10% reduction from experimental value $a/L_{Ti} = 3.918$.

maximum during the linear start-up phase. This phase is not useful for comparisons with experiments. Depending on the specific case, the simulation times-step is sometimes reduced during the linear start-up phase to resolve the rapid changes in heat flux. After the linear start-up phase, there are relatively large heat fluxes in the time period $50 < t < 200\,a/c_s$ when the turbulence is driven strongly, because the E×B shear is still off and the ion temperature gradient is set to the measured experimental value. At $t = 200a/C_s$, the E×B shear effects are turned on and the parameter a/L_{Ti} is reduced 26.25% from the starting value.

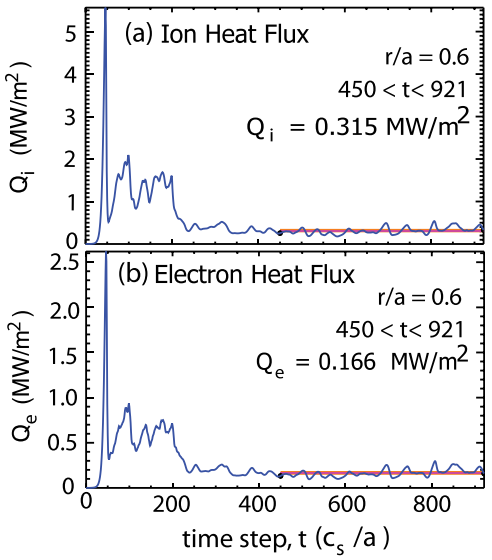

FIG. 3. The ion heat flux (a) and electron heat flux (b) output from the local GYRO simulation at $r/a = 0.6$ for L-mode are shown as a function of simulation time-step.

The simulation is allowed to run another 250 time steps to ensure a steady phase is reached. After a steady phase is reached, the simulation results are averaged over time periods of typically 400–500 time steps to obtain an average value for comparison with the experimental heat fluxes. In this L-mode case for the simulation at $r/a = 0.6$, the time period $450 < t(a/C_s) < t_{max}$, where $t_{max} = 921$ is used for the average. The red line indicates the average simulation ion and electron heat flux values, which are $Q_i = 0.315$ MW/m^2 and $Q_e = 0.166$ MW/m^2, respectively. Once a simulation has been run with the experimental values as input, the output ion heat flux is compared to the experimental values. If there is disagreement, only one input parameter, the normalized ion temperature gradient scale length, a/L_{Ti}, is varied within error bars to try to match the ion heat flux output with experiment (giving the "heat flux-matched" simulation). This approach has been used successfully for C-Mod plasmas previously.[38] Sections III B–III D describe the output of the heat flux-matched simulations and comparisons with experiments.

B. Comparison of GYRO predicted heat fluxes with experimental heat fluxes

It is important to examine the wavenumber spectrum of the simulated heat fluxes to determine if significant

contributions to heat flux exist at the highest wavenumber resolved, and to check that the smallest wavenumber simulated is well resolved. In Fig. 4, ion heat flux (a) and electron heat flux (b) output from the local GYRO simulation at $r/a = 0.6$ for L-mode (green) are shown as a function of simulated $k_\theta \rho_s$. The lower panels show the ion heat flux (c) and electron heat flux (d) for I-mode (purple). There is no difference between L-mode and I-mode in shape of the spectra at $r/a = 0.6$ for ion or electron heat flux. In both simulations, there is insignificant electron heat flux driven at the highest simulated wavenumber, and the low wavenumbers are well resolved.

In contrast to the simulations run at $r/a = 0.6$, simulations run at $r/a = 0.8$ do show roughly 10% contributions to the heat flux from the short wavelength modes, $k_\theta \rho_s > 1$. Figure 5 shows the ion heat flux (a) and electron heat flux (b) output from the local GYRO simulation at $r/a = 0.8$ for L-mode (green) as a function of simulated $k_\theta \rho_s$; and the ion heat flux (c) and electron heat flux (d) are shown for I-mode (purple). There is 13% of the total heat flux driven at high k ($k_\theta \rho_s > 1$) in L-mode and 10% in I-mode. Compared to the

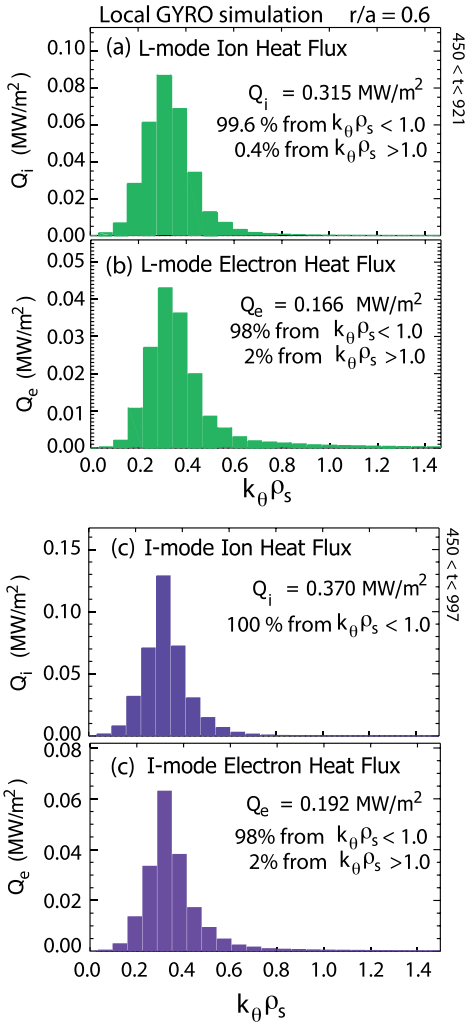

FIG. 4. The ion heat flux (a) and electron heat flux (b) output from the local GYRO simulation at $r/a = 0.6$ for L-mode (green) are shown as a function of simulated $k_\theta \rho_s$. The bottom panels show ion heat flux (c) and electron heat flux (d) for I-mode (purple). There is no difference between L-mode and I-mode in shape of the spectra.

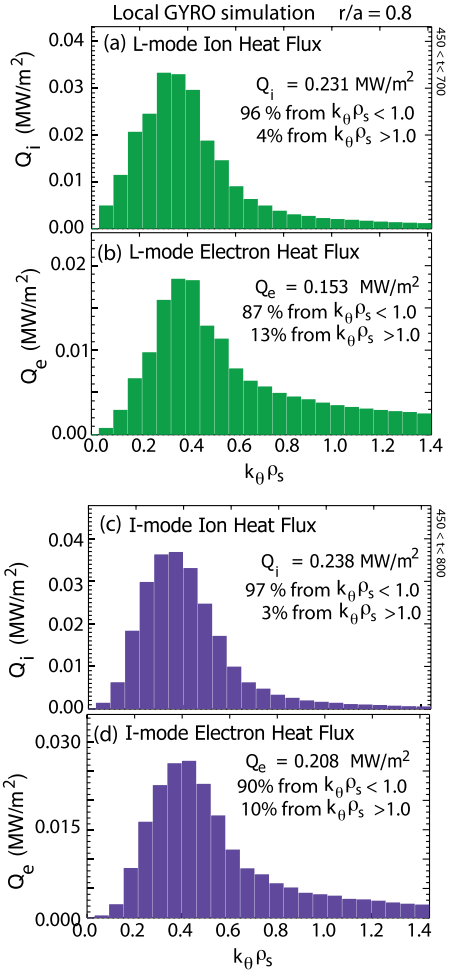

FIG. 5. The ion heat flux (a) and electron heat flux (b) output from the local GYRO simulation at $r/a = 0.8$ for L-mode (green) are shown as a function of simulated $k_\theta \rho_s$, and below the ion heat flux (c) and electron heat flux (d) are shown for I-mode (purple). The shape of the spectra at r/a = 0.8 for electron heat flux is very similar between L-mode and I-mode, with 13% of the total heat flux driven at high k ($k_\theta \rho_s > 1$) in L-mode compared with 10% in I-mode.

simulations at inner radii, such as $r/a = 0.6$, there is generally more heat flux driven at higher wavenumber at outer radii. We note that similar to the results at $r/a = 0.6$, there is no shift of the peak of the spectrum from L-mode to I-mode, and no change in shape at $r/a = 0.8$.

Figure 6 shows the experimental heat fluxes compared with results from local heat flux-matched GYRO simulations at two radial locations. The solid black lines are the experimental heat flux values, and the dashed black lines represent the 1 sigma error bars. The purple triangles are results from I-mode and green circles are results from L-mode. Figures 6(a) and 6(b) show that the ion and electron heat flux could be matched simultaneously in I-mode at both radial locations. The solid triangles are results when only a/L_{Ti} is modified match ion heat flux. At the inner radial location in I-mode, we found that an additional small increase in a/L_{Te} of 7.5% that is within experimental error would increase the ion heat flux to better match experiment (not shown here), without impacting the agreement in the electron heat flux. In contrast to I-mode, where both ion and electron heat fluxes were matched simultaneously, Figs. 6(c) and 6(d) show that

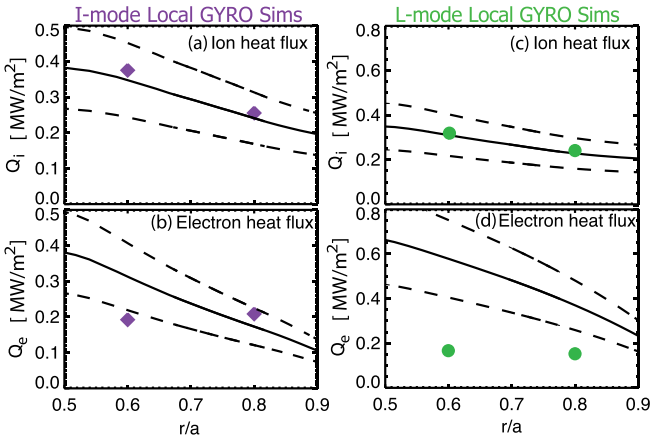

FIG. 6. Experimental heat fluxes compared to results from local GYRO simulations at two radial locations. The solid black lines are the experimental heat flux values, and the dashed black lines represent the 1 sigma error bars. The purple triangles are results from I-mode and green circles are results from L-mode. Panels (a) and (b) shown that the ion and electron heat flux can be matched simultaneously in I-mode at both radial locations. Panels (c) and (d) show that in L-mode, ion heat flux can me matched, but electron heat flux is underpredicted.

in L-mode, ion heat flux could be matched with only changes in a/L_{Ti}, but electron heat flux is under predicted. No changes of other input parameters within error bars gave better agreement with the electron heat flux. The L-mode plasma provides another example of underprediction of electron heat flux commonly observed with ion-scale simulations in C-Mod L-mode plasmas.[28]

C. Stiffness scans

While the ion heat flux-matched simulations were used for direct comparisons with the experiment, we performed wider scans of input gradients in order to map out flux-gradient space and identify differences in critical gradient and profile stiffness between L-mode and I-mode. A first definition of temperature profile stiffness can be "the degree of sensitivity of the heat flux to the driving gradient," a definition that has been used for recent gyrokinetic simulation studies of JET plasmas.[23] This definition uses the fact that the turbulence is driven unstable by logarithmic temperature gradients that are above a critical threshold and is related to the incremental diffusivity. In a plot of heat flux, Q, vs normalized temperature gradient scale length, a/L_T, there will be a critical gradient $a/L_{T,crit}$, below which little heat flux is driven (an x-intercept). Above the critical gradient, the change in heat flux with gradient can be defined as the stiffness, $S = dQ/dz$. Typically, in this definition, Q is the ion heat flux and $z = a/L_{Ti}$ is the normalized ion temperature gradient scale length in the case of Ion Temperature Gradient (ITG) turbulence at fixed temperature,[16] but a critical gradient and stiffness can also exist for density and electron temperature gradients, which are relevant for different turbulent modes.[39] A second definition of stiffness can be "the measure of nearness to the critical gradient," and the stiffness could be written as $S = d\ln(Q)/d\ln(z) = (z/Q)\,dQ/dz$ (where again, Q is the ion heat flux and $z = a/L_{Ti}$ is the normalized ion temperature gradient scale length). As a/L_{Ti} approaches $a/L_{Ti,crit}$ and the heat flux Q becomes very small, then S as defined above will tend to infinity. This will be true regardless of how the heat flux responded to changes in the driving gradient above threshold. Stiffness is therefore also a measure of how close the profile is to marginal stability. We note that there are additional ways to characterize stiffness, and different ways to include the effect in transport models; we refer the reader to the following article (and references therein) for discussion.[14]

Figure 7 shows the simulated ion and electron heat fluxes plotted against input parameter a/L_{Ti} at $r/a = 0.6$. The critical gradient in a/LTi is the point where the ITG driven heat flux in the simulation is zero because the ITG is stabilized. For L-mode, the critical gradient value at $r/a = 0.6$ is $a/L_{Ti,crit}/approx2.0$ and in I-mode, $a/L_{Ti,crit} \approx 1.8$. We note that in general there can be residual transport driven by other modes, such as TEM, below the critical gradient. However, for these plasmas, the ITG mode is dominant and near the critical gradient the heat flux driven in the simulations becomes negligible, close to zero, with no residual transport. The value of a/L_{Ti} used as input to the simulations that matches the experimental ion heat flux at $r/a = 0.6$ in the I-mode plasma, $a/L_{Ti,match} = 1.85$, is only $\approx$3% above the critical gradient, which means that the ion temperature profile very close to marginal stability. In contrast, the value of $a/L_{Ti,match} = 2.20$ used as input to the simulations that matches the experimental ion heat flux at $r/a = 0.6$ in the L-mode plasma is 10% above the critical gradient, farther from marginal stability. Figure 7 also shows the differences in the incremental heat flux between L-mode (green) and

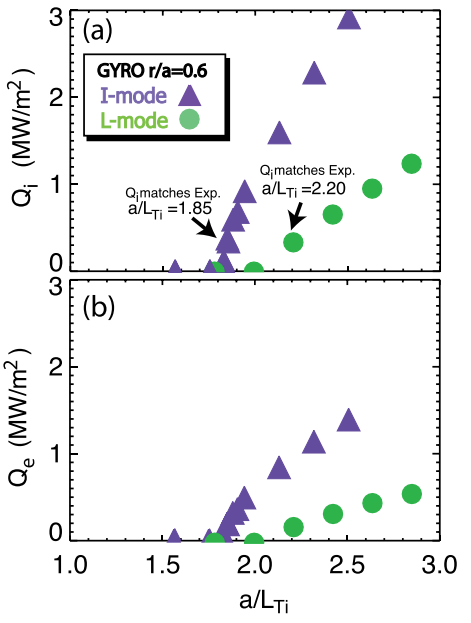

FIG. 7. Results from scans of the GYRO input a/L_{Ti} at $r/a = 0.6$. The ion heat flux in experimental units, MW/m^2, is plotted versus a/L_{Ti}. In these units, the incremental heat flux (slope of the line above the critical gradient) is lower in L-mode (green) than in I-mode (purple). This plot shows that I-mode is more stiff than L-mode (according to both definitions: incremental response to a change in gradient and nearness to marginality). I-mode is closer to marginal stability than L-mode, since the heat flux matching value of a/L_{Ti} is only 3% above the critical value in I-mode but is 10% above in L-mode.

I-mode (purple). Considering only values of a/L_{Ti} above the critical gradient, the slope of the straight line fit through the simulation data points gives the stiffness related to the incremental heat flux, according to the first definition. The simulations show that the I-mode ion temperature profile is more stiff (steeper slope) than L-mode. By either definition of stiffness, "the degree of sensitivity of the heat flux to the driving gradient" or "the measure of nearness to the critical gradient," the GYRO simulations show that the I-mode ion temperature profile at $r/a = 0.6$ is more stiff than the L-mode ion temperature profile. Figure 7 shows the simulated ion and electron heat fluxes plotted against input parameter a/L_{Ti} at $r/a = 0.8$. For L-mode, the critical gradient value at $r/a = 0.8$ is higher than in I-mode. Again, considering only values of a/L_{Ti} above the critical gradient, the slope of the straight line fit through the simulation data points shows that the I-mode ion temperature profile is more stiff (steeper slope) than L-mode. The a/L_{Ti} scan at $r/a = 0.8$ shows similar results to $r/a = 0.6$: the I-mode ion temperature profile is more stiff than the L-mode ion temperature profile (Fig. 8).

We also scanned the input value of a/L_{Te} to probe stiffness and critical gradient with respect to the electron temperature profile. Results from scans of a/L_{Te} at $r/a = 0.6$ and $r/a = 0.8$ are shown in Figs. 9 and 10, respectively. The scans are performed around the ion heat flux-matched cases (e.g., at fixed a/L_{Ti}). Figure 9 shows that at $r/a = 0.6$ in L-mode and I-mode the ion heat flux responds very little to changes in *a/LTe*, except for the lowest value of a/L_{Te}, which stabilized the turbulence in the I-mode simulation. In contrast, the electron heat flux does respond to changes in a/L_{Te}, but less so than when a/L_{Ti} is varied. This is consistent with the turbulence being dominated by ITG-mode characteristics. Scans of input a/L_{Te} were also performed around the heat flux-matched simulations at $r/a = 0.8$. The ion and electron heat flux plotted vs a/L_{Te} are shown in Fig. 10.

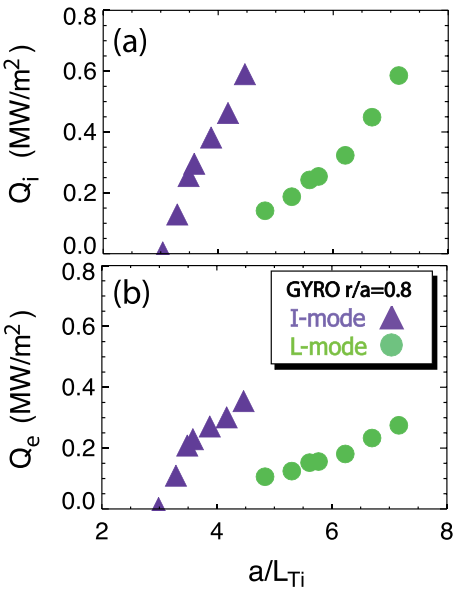

FIG. 8. Results from scans of the GYRO input a/L_{Ti} at $r/a = 0.8$. The scans show that I-mode is more stiff than L-mode, I-mode has a lower critical gradient in a/L_{Ti}, and I-mode is closer to marginal stability, similar to the findings for $r/a = 0.6$.

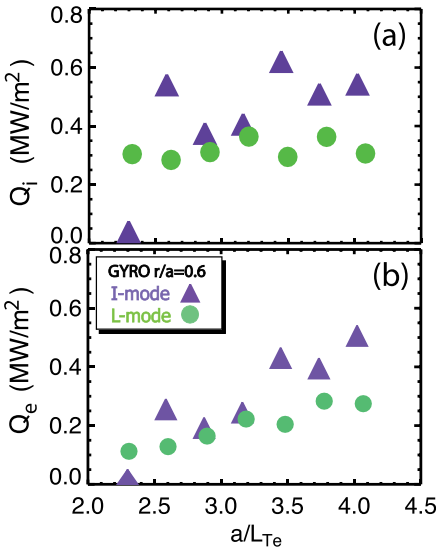

FIG. 9. GYRO scans in a/L_{Te} are shown at $r/a = 0.8$. The scans are performed around the ion heat flux-matched cases (e.g., at fixed a/L_{Ti}). The ion and electron heat flux plotted vs a/L_{Te}. As shown in panel (a) in both L-mode and I-mode ion heat flux resounds very little to changes in *a/LTe*, except for the lowest value of *a/LTe*, which stabilized the turbulence in I-mode. In contrast, panel (b) shows that the electron heat flux does respond weakly to changes in a/L_{Te}. The stiffness for electron temperature in I-mode is higher than in L-mode, but the stiffness is not as large as what is observed the ion temperature.

Panel (a) shows that ion heat flux in both L-mode and I-mode decreases as a/L_{Te} is increased. Panel (b) shows that I-mode exhibits small but finite stiffness and electron heat flux increases as temperature gradient increases, but L-mode shows no stiffness (a flat response). The a/L_{LTe} scans in the simulations show that electron temperature profile is more stiff in I-mode is higher than in L-mode at both radial locations $r/a = 0.6$ and $r/a = 0.8$. However, the a/L_{LTe} scans in

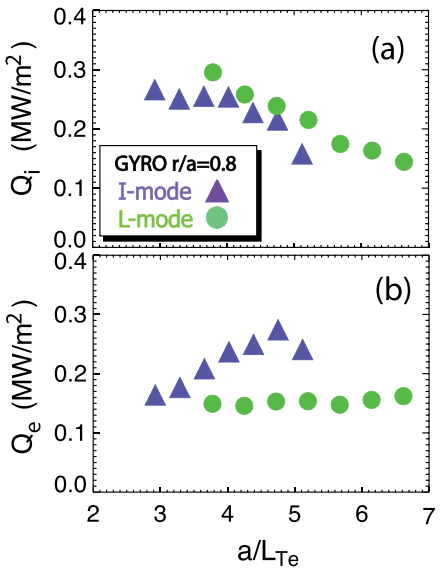

FIG. 10. GYRO scans in a/L_{Te} are shown at $r/a = 0.8$. The scans are performed around the ion heat flux-matched cases (e.g., at fixed a/L_{Ti}). Panel (a), both L-mode and I-mode ion heat flux decreases in response to increases in a/L_{Te}. Panel (b) shows that I-mode exhibits small but finite stiffness and electron heat flux increases as temperature gradient increases, but L-mode shows no stiffness (a flat response).

the simulations show that the electron temperature profile stiffness is rather weak in both L-mode and I-mode (contrasted with the ion temperature profile). This result from the simulation is in disagreement with general experimental observations at C-Mod, where the measured electron temperature profile in the core plasma strongly exhibits self-similarity,[40] which is an indication of nearness to marginality, and of high stiffness. The caveat with these simulation results is that the simulations only include ion-scale turbulence. The electron temperature stiffness predicted by ion-scale and multi-scale simulations can be different if Electron Temperature Gradient (ETG) makes large contributions to the heat flux, as has been suggested by recent work,[29] and such simulations may show better agreement with general experimental observations of electron temperature profile stiffness.

D. Effect of $E \times B$ shearing rate

Even though the C-Mod plasmas have no external momentum input, and all rotation is intrinsic rotation, we found that including the effect of the $E \times B$ shearing in the simulations was necessary to obtain agreement with experimental heat fluxes. In L-mode and I-mode plasmas, the $E \times B$ shearing rate is similar in both L-mode and I-mode at both radii, with $\gamma_{E\times B} = 0.042$ and 0.035 (c_s/a) at $r/a = 0.6$ in L-mode and I-mode, respectively, and $\gamma_{E\times B} = 0.080$ and 0.083 (c_s/a) at $r/a = 0.8$ in L-mode and I-mode, respectively. Even in plasmas with similar shearing rates, the effect of the shearing can be different, depending on how strongly the turbulence is driven. To assess whether or not the turbulence responds similarly in L-mode and I-mode, scans of the $E \times B$ shearing rate were performed about the ion heat flux-matched cases (GYRO inputs are shown in Table I), with all other parameters held fixed. Figure 11 shows the results of scans of the $E \times B$ shearing rate in GYRO in both L-mode and I-mode at $r/a = 0.6$. A scaling factor of 0 corresponds to the experimental value, factors of ± 0.30 correspond to increased/decreased shear by 30%. Figures 11(a) and 11(b) show that when $E \times B$ shearing rate was increased in the simulations, the turbulence is fully suppressed in both L-mode and I-mode. In I-mode (purple), when $E \times B$ shear was decreased by 30% there was roughly a factor of 2 increase in both the ion and electron heat fluxes. In contrast to the large response in I-mode, when $E \times B$ was decreased by 30% in L-mode (green), the ion heat flux increased ≈16% and electron heat flux increased ≈18%. These scans suggest that the $E \times B$ shear suppression of core turbulence, while present in both L-mode and I-mode conditions, has a larger effect on transport in I-mode than in L-mode. Results from the $E \times B$ shear scans were similar at the outer radius, $r/a = 0.8$. Finer scans of the shearing rate are planned for future work to investigate the effects of increasing $E \times B$ shear without fully suppressing the turbulence. In addition, at different $E \times B$ shear values, the stiffness can change,[23] so future work will also include wider sets of scans to investigate this effect.

To connect with past work at C-Mod[8] and with general understanding of the $E \times B$ shear suppression in plasmas,[41] we compared linear growth rates to $E \times B$ shearing rates in Fig. 12. The linear stability analysis is performed using the flux-matched values of a/LTi listed in Table I. The range of the experimental $E \times B$ shear values is indicated as the red shaded bar in Fig. 12. For both L-mode and I-mode, the dominant linear instability was an ITG-type mode and there is very little difference in the growth rate between L-mode and I-mode. In addition, linear growth rates in both L-mode and I-mode are higher than the $E \times B$ shearing rate at most low-k values. This contrasts with the results of previous linear stability analysis published for these same plasmas.[8] The

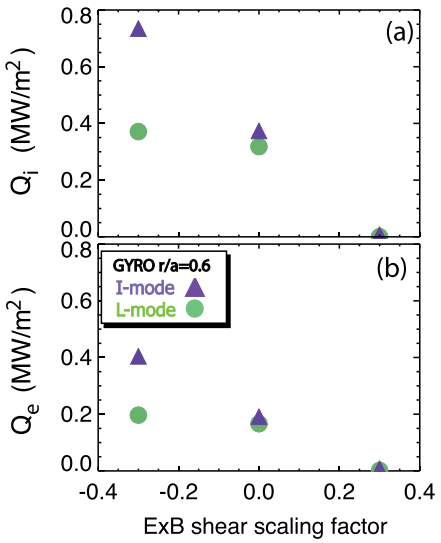

FIG. 11. Scans of the $E \times B$ shearing rate in GYRO. $E \times B$ shearing rate scaling factor, which is first set at 0 corresponding to the experimental value for the first simulation, and is decreased 30% and increased 30% in two other simulations. For I-mode (purple triangles), when $E \times B$ shear is decreased, there is a large increase in heat fluxes. In contrast, at lower values of $E \times B$ shear, the L-mode shows a weaker increase in heat fluxes compared with I-mode.

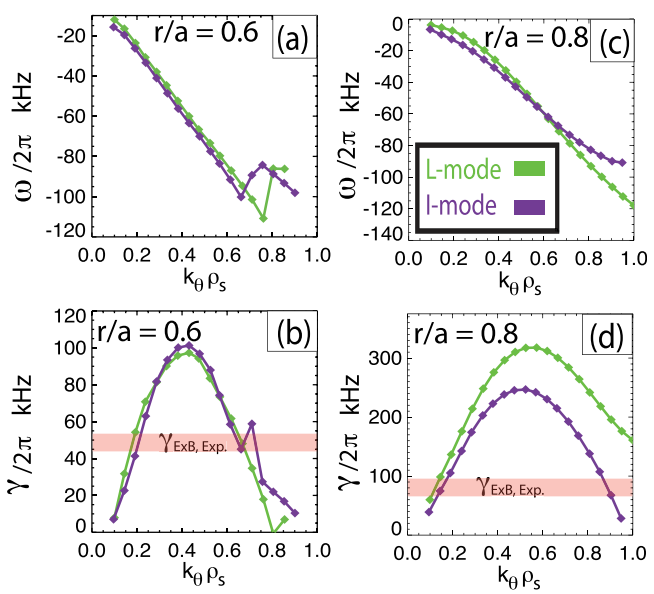

FIG. 12. Results from linear stability analysis, with GYRO, performed using the ion heat flux-matched parameters (Table 1) as input. Panel (a) and (b) show the real frequency of the fastest growing mode vs $k_\theta \rho_s$ and the growth rate vs $k_\theta \rho_s$, respectively, at $r/a = 0.6$. I-mode is purple and L-mode is green.

difference is due to different input profiles used for the linear GYRO analysis. In the previous paper,[8] the linear stability analysis was run with the experimental profiles (experimental values of a/L_{Ti}, see footnotes in Table I). For those input parameters, the growth rate decreased in I-mode compared to L-mode and becomes comparable to the $E \times B$ shearing rate over most of the range $0 < k_\theta \rho_s < 1$. When the ion heat flux-matched values of a/L_{Ti} are used, the result is shown in Fig. 12, where the linear growth rates in I-mode are above the $E \times B$ shearing rate for many values of wavenumber $k_\theta \rho_s$.

IV. COMPARISONS OF REDUCED EXPERIMENTAL FLUCTUATION LEVELS WITH GYRO

In the experimental discharge simulated with GYRO in this paper, the core long wavelength ($k_\theta \rho_s < 0.5$) density fluctuations were measured with a reflectometer diagnostic in both L-mode and I-mode. In different L-mode and I-mode plasmas, the long wavelength ($k_\theta \rho_s < 0.3$) electron temperature fluctuations were measured with a Correlation ECE (CECE) diagnostic at C-Mod. Details of the measurement set-up and analysis are described in Ref. 8. Figure 13 shows the experimental percent reduction in measured relative density and temperature fluctuation amplitudes compared to the results from local GYRO simulations at two radial locations. The solid symbols are the experimental percent reductions (going from L-mode to I-mode) in density (blue) and electron temperature fluctuation amplitudes (red). The open symbols are the GYRO percent reductions in the relative fluctuation levels. In the experiment, the density fluctuation level decreased by $\approx 30\%$ at $r/a = 0.6$ and $\approx 20\%$ at $r/a = 0.8$ in I-mode compared to L-mode. The GYRO simulations predicted $\approx 30\%$ reductions in long wavelength density fluctuation amplitude in the simulations at both radii, which is consistent with the experimental observations. For temperature fluctuations, the simulations predicted reductions of less than 10% at both radii. This is smaller than the experimentally measured reductions (with are at least 50%) at $r/a = 0.8$. In the experiment, the CECE measured fluctuation levels inside $r/a = 0.7$ were below the diagnostic noise limit in both L-mode and I-mode, so no fluctuations (and therefore no reductions) could be measured deeper in the core during these experiments.

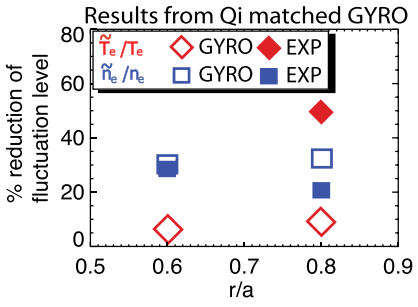

FIG. 13. The experimental percent reduction in measured density and temperature fluctuation amplitudes compared to results from local GYRO simulations at two radial locations. The solid symbols are the experimental percent reductions in density (blue) and electron temperature fluctuation amplitudes (red). Open symbols are simulation results.

V. DISCUSSION

This paper has presented the first nonlinear gyrokinetic simulations of I-mode plasmas with comparisons to experiments from Alcator C-Mod. I-mode is a high confinement regime, featuring energy confinement similar to H-mode, but without enhanced particle and impurity particle confinement.[1] We have found that standard, long wavelength nonlinear gyrokinetic simulations (with the GYRO code) agree well with experimental characteristics of I-mode. However, some discrepancies between GYRO and experimental characteristics remain outstanding and will be investigated as part of future work.

There are several open questions that go beyond the scope of this paper, which are left to future work. First, the most striking thing about the turbulent transport in I-mode is the natural separation of heat and particle transport that is observed experimentally. We have performed experiments at C-Mod on impurity transport and particle transport in I-mode, for comparisons with L-mode and H-mode.[42] Future simulation work will explore the particle transport using these data sets. We plan to make direct comparisons between nonlinear GYRO simulation results and measured impurity particle transport using established techniques.[43]

Second, in contrast to the I-mode results where both experimental ion and electron heat flux can be matched with long wavelength simulations, there remains a robust underprediction of electron heat flux in the L-mode plasmas that must be understood. We have attributed this to the absence of electron scale turbulence in the simulations, suggesting that the missing electron heat flux is caused by ETG contributions. This is especially important because electron heat flux-matched simulations are needed to probe the stiffness of the electron temperature profile accurately. Using the first ever multi-scale ($0 < k_{theta}\rho_s < 48$) realistic mass ratio ($\sqrt{M_i/m_e} = 60$) gyrokinetic simulations of deuterium tokamak plasmas,[29] it has been shown that GYRO simulations of ITG-TEM-ETG turbulence simultaneously match the electron and ion heat flux in L-mode plasmas at C-Mod. Those new results suggest that ETG plays a much more critical role in determining both electron and ion heat flux (due to enhancements caused by the ETG-ITG coupling) in the core of L-mode plasmas than was previously thought. Linear stability analysis shows that ETG is unstable in both the L-mode and I-mode plasmas here. Future work on understanding the role of ETG turbulence in C-Mod L-mode and I-mode plasmas will be pursued with advanced simulations of existing data sets as well as with new experiments.

Third, the nonlinear GYRO simulations we present here do show gyroBohm transport in I-mode and do suggest that most of the core transport physics in the I-mode is consistent with our standard picture of core turbulent transport which is important to establish. As a consequence of the gyroBohm transport in I-mode and L-mode, the incremental heat flux (slope of the line above the critical gradient) is the same in both plasmas when the ion heat flux is in gyroBohm units, Q_i/Q_gB, as shown in Fig. 14. Related to this, in the ion-heat flux-matched simulations at $r/a = 0.6$ the simulated turbulence correlation lengths are very similar in normalized

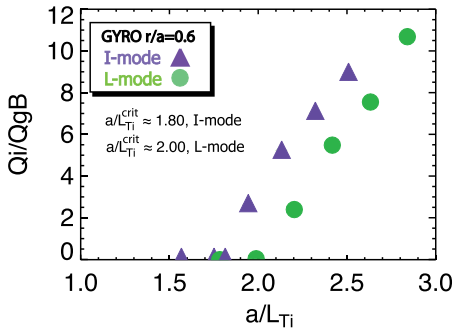

FIG. 14. Results from scans of the GYRO input a/L_{Ti} at $r/a = 0.6$. The ion heat flux is plotted in gyroBohm units versus a/L_{Ti}. In these units, the incremental heat flux (slope of the line above the critical gradient) is the same in both L-mode (green) and I-mode (purple). This plot still shows that I-mode is more stiff than L-mode (according to the definition of nearness to marginality), since changing units does not change the critical gradient. I-mode is closer to marginal stability than L-mode, since the heat flux matching value of a/L_{Ti} is only 3% above the critical value in I-mode, but is 10% above in L-mode.

gyroBohm units. This is consistent with the idea that the hotter plasma is more stiff due to the larger turbulence eddy length scales. To probe this deeply would require an extensive set of simulations and experiments that are beyond of the scope of this paper. For reference, Table II lists the predicted turbulence parameters at $r/a = 0.6$ from the ion heat flux-matched GYRO simulations presented here. The turbulence quantities from the simulation are taken at the outboard midplane, are box averaged over the time range specified in the table, and represent an average over all the wavenumbers in simulation (i.e., no attempt at synthetic diagnostic filtering was performed).

Fourth, in addition to further study of the correlation lengths, we are pursuing direct comparisons between GYRO and the measured electron temperature fluctuations using synthetic diagnostics[44] to better understand the differences between the measured percent reduction and the predicted reduction. It would also be fruitful to use a synthetic reflectometer diagnostic in future work to compare directly with GYRO. Other fluctuation measurements, such as Phase Contrast Imaging (PCI)[45] and fast two color interferometer (FTCI),[46] can also be used to further study the turbulent transport in I-mode plasmas at C-Mod.

Fifth, we are interested in examining perturbative transport in I-mode by following the propagation of heat pulses due to sawteeth[47] and also through the use of cold-pulse experiments.[48] Examining experimentally the differences between the stiffness inferred from the pulse propagation (which is related to the incremental diffusivity) and the power balance values is important. There may be a relationship between the reported high values of the perturbative thermal diffusivity and the strength of the ETG transport. However, the heat pulse analysis can be difficult to interpret, so this is left for a dedicated future project.

TABLE II. This table contains output parameters of interest from the ion heat flux-matched local GYRO simulations at $r/a = 0.6$, taken from long time averages, $>450a/c_s$, during the steady period of the simulations.

Local parameter	L-mode r/a = 0.6	I-mode r/a = 0.6
Time range (c_s/a)	450–921	450–997
c_s (m/s)	2.531e5	3.112e5
Q_{gB} (MW/m^2)	0.121	0.336
χ_{gB} (m^2/s)	0.516	0.958
$k_y\rho_s^{max}$	1.434	1.466
Q_i^{sim} (MW/m^2)	0.318	0.375
Q_e^{sim} (MW/m^2)	0.166	0.192
Q_i^{sim}/Q_i^{gB}	2.628	1.116
$Q_e^{sim}Q_e^{gB}$	1.372	0.571
Q_i^{sim}/Q_i^{exp}	1.026	1.081
Q_e^{sim}/Q_e^{exp}	0.288	0.615
$\delta\phi/eT_e$	1.07%	0.93%
$\delta n_e/n_e$	0.90%	0.63%
$\delta T_e/T_e$	0.79%	0.74%
$\delta T_i/T_i$	1.46%	1.13%
$^{\delta\phi/eT_e}L_{rad}/\rho_s$	8.97	9.22
$^{\delta n_e/n_e}L_{rad}/\rho_s$	8.31	8.56
$^{\delta T_e/T_e}L_{rad}/\rho_s$	7.84	7.94
$^{\delta T_i/T_i}L_{rad}/\rho_s$	8.26	8.27

VI. SUMMARY AND CONCLUSIONS

Comparisons with long wavelength, ion-scale local GYRO simulations showed that ion and electron heat flux could be matched simultaneously in I-mode at both $r/a = 0.6$ and $r/a = 0.8$ with only modifications of a/L_{Ti} within experimental error bars. In contrast, for L-mode the ion heat flux could be matched, but electron heat flux was under predicted. This result in L-mode plasmas is generic to C-Mod and is apparently unrelated to the DIII-D transport shortfall.[28,37] The missing electron heat flux in GYRO simulations of L-mode plasmas in C-Mod seems to be related to high-k ETG contributions that are not included in the type of simulations used in this paper. Recent validation work at C-Mod has shown that multi-scale realistic mass simulations of coupled ITG/TEM/ETG turbulence can match the L-mode electron heat flux levels.[29] Multi-scale simulations of I-mode plasmas are part of future work.

Scans of the input $E \times B$ shear in the local nonlinear GYRO simulations suggest that the $E \times B$ shear suppression of core turbulence, while present in both L-mode and I-mode conditions, has a larger effect on transport in I-mode than in L-mode. Finer scans of the shearing rate in nonlinear simulations are planned for future work to investigate the effects of increasing $E \times B$ shear without fully suppressing the turbulence. In addition, at different $E \times B$ shear values the stiffness can change,[23] so future work will also include wider sets of scans to investigate this effect.

While the ion heat flux-matched simulations were used for direct comparisons with the experiment, wider scans of input a/L_{Ti} and a/L_{Te} around the flux-matched simulations were performed. These GYRO scans showed that I-mode is more stiff than L-mode and has a lower critical gradient in a/L_{Ti} than L-mode, with the result that I-mode is much closer to marginal stability than L-mode. This has consequences for the expected fidelity of profile prediction, with models like TGLF.

Long wavelength density fluctuations ($k_\theta\rho_s < 0.5$) were measured with a reflectometer diagnostic, and electron

temperature fluctuations ($k_\theta \rho_s < 0.3$) were measured with a CECE diagnostic at C-Mod. Measured fluctuations in the core plasma were reduced across the L-I transition. In the experiment, the density fluctuation level decreased by ≈30% at $r/a = 0.6$ and ≈20% at $r/a = 0.8$ in I-mode compared to L-mode. The GYRO simulations predicted ≈30% reductions in long wavelength density fluctuation amplitude in the simulations at both radii, which is consistent with the experimental observations. We plan in future work to apply synthetic reflectometer diagnostics to the simulations presented in this paper to make more direct comparisons with the measured density fluctuation levels.

For temperature fluctuations, the simulations predicted reductions of less than 10% at both radii. This is smaller than measured reductions in I-mode, which are at least 50% at $r/a = 0.8$.[8] The discrepancy could be related to the missing electron heat flux in L-mode, since we are comparing the ratio of L-mode to I-mode fluctuation levels. However, it could also be due to differences between the experimental conditions and the simulated conditions, since the electron temperature fluctuations were not measured in the same plasmas as the density fluctuations. Work is in progress to use GYRO to simulate the plasmas where partial profiles of electron temperature fluctuations were measured.[8] This will allow for quantitative comparisons of GYRO results with temperature fluctuation levels, using a synthetic CECE diagnostic.[37]

While there was reasonably good agreement with the measured trend in density fluctuation level reduction, the discrepancy with the electron temperature fluctuation reduction could be due to a number of things. First, the missing electron heat flux in L-mode affects the comparison made here, because the ratio between L-mode and I-mode is compared to simulations. Second, there can be slight differences between the experimental conditions and the simulated conditions, since the electron temperature fluctuations were not measured in the same plasmas as the density fluctuations. Third, while the wavenumber sensitivities of the reflectometer and CECE should not affect the GYRO comparisons in this paper (because we compare only the ratio of fluctuation levels in I-mode and L-mode), it could have an effect and will be probed with future synthetic diagnostic modeling. Fourth, including the effects of ETG contributions in future simulations is expected to improve comparisons with the electron heat flux, but it is not clear if this will change predictions for the fluctuation levels at long wavelength.

In previous work from Alcator C-Mod,[8] we speculated that reduced fluctuation levels in the core of I-mode plasmas could be a result of both changing $E \times B$ shear suppression[41] and changing stiffness. The nonlinear GYRO simulation results presented here are consistent with this. The series of flux-gradient scans showed that temperature profiles in the I-mode core plasmas are more stiff than in L-mode core plasmas. Scans of the input $E \times B$ shear in GYRO simulations showed that reduced $E \times B$ shearing has a stronger effect in the core of I-mode than L-mode. The nonlinear simulations match the observed reductions in long wavelength density fluctuation levels across the L-I transition, but underestimate the reduction of long wavelength electron temperature fluctuation levels. We conclude that the increased $E \times B$ shearing of turbulence combined with increased profile stiffness can account the reductions in core turbulence reported previously.[8] This is significant because it indicates that I-mode plasmas feature "stiff" core transport properties similar to what is generally observed in H-modes. These new nonlinear GYRO simulation results are important when considering I-mode plasmas as a target for operation in ITER and other future experiments. The role of $E \times B$ shear suppression in determining the improved confinement in I-mode is also significant, because at C-Mod, the plasma rotation is intrinsically generated (not driven by neutral beam injection). The new results from the nonlinear GYRO simulations presented here suggest that intrinsic rotation shear can suppress core turbulence in high performance plasmas. There was evidence of this in ITB plasmas previously at C-Mod,[49] but this is the first evidence for the effect in a general high confinement mode core plasma without an ITB.

Overall, the first comparisons between I-mode plasmas and nonlinear GYRO simulations provide evidence that existing gyroknetic and gyrofluid transport models can be used to predict performance in I-mode plasmas. Because long wavelength simulations can match both the ion and electron heat flux in I-mode, and since I-mode is found to be quite stiff and near marginal stability, reduced models, such as TGLF, would be expected to work well in I-mode plasmas at C-Mod. Preliminary TGLF modeling of the discharge 1 101 209 029 (not shown here) does show reasonably good agreement with experiment. More work is needed, since it will be useful to compare nonlinear gyrokinetic codes to a wide data base of I-mode plasmas, from C-Mod, ASDEX, and DIII-D.

ACKNOWLEDGMENTS

We wish to acknowledge the outstanding expertise and support of the Alcator C-Mod team of scientists, engineers, and technicians at MIT, without whom these experiments would not have been possible. Experimental data sets were collected at the Alcator C-Mod tokamak, a DOE Office of Science user facility, supported by DOE Contract No. DE-FC02-99ER54512-CMOD. The nonlinear gyrokinetic calculations with the GYRO code were performed using the National Energy Research Scientific Computing Center, which was supported by the Office of Science of the U.S. Department of Energy under Contract No. DE-AC02-05CH11231.

[1]D. G. Whyte, A. E. Hubbard, J. W. Hughes, B. Lipschultz, J. E. Rice, E. S. Marmar, M. Greenwald, I. Cziegler, A. Dominguez, T. Golfinopoulos, N. Howard, L. Lin, R. M. McDermott, M. Porkolab, M. L. Reinke, J. Terry, N. Tsujii, S. Wolfe, S. Wukitch, Y. Lin, and the Alcator C-Mod Team, Nucl. Fusion **50**, 105005 (2010).

[2]J. R. Walk, J. W. Hughes, A. E. Hubbard, J. L. Terry, D. G. Whyte, A. E. White, S. G. Baek, M. L. Reinke, C. Theiler, R. M. Churchill, J. E. Rice, P. B. Snyder, T. Osborne, A. Dominguez, and I. Cziegler, Phys. Plasmas **21**, 056103 (2014).

[3]A. E. Hubbard, D. G. Whyte, R. M. Churchill, I. Cziegler, A. Dominguez, T. Golfinopoulos, J. W. Hughes, J. E. Rice, I. Bespamyatnov, M. J. Greenwald, N. Howard, B. Lipschultz, E. S. Marmar, M. L. Reinke, W. L. Rowan, J. L. Terry, and A. C.-M. Group, Phys. Plasmas **18**, 056115 (2011).

[4]A. E. Hubbard, D. G. Whyte, R. M. Churchill, A. Dominguez, J. W. Hughes, Y. Ma, E. S. Marmar, Y. Lin, M. L. Reinke, and A. E. White, Nucl. Fusion **52**, 114009 (2012).
[5]F. Ryter, R. M. McDermott, T. Putterich, J. Vicente, E. Viezzer, E. Wolfrum, C. Angioni, M. Bernert, J. C. Boom, R. Fischer, B. Geiger, S. da Graca, B. Kurzan, N. C. Luhmann, Jr., H. K. Park, S. K. Rathgeber, P. Sauter, M. Villensdorfer, and the ASDEX Upgrade Team, *Paper presented at the 38th Annual European Physical Society Conference on Plasma Physics Strasbourg, Germany* (2011), p. P5.112.
[6]A. E. Hubbard, T. Osborne, F. Ryter, X. Gao, J. Ko, L. B. Orte, R. M. Churchill, I. Cziegler, M. Fenstermacher, R. Fischer, S. Gerhardt, R. Groebner, P. Gohi, T. Happel, J. W. Hughes, Z. X. Liu, A. Loarte, R. Maingi, A. Marinoni, E. S. Marmar, R. M. McDermott, G. McKee, T. Rhodes, J. E. Rice,, L. Schmitz, C. Theiler, E. Viezzer, J. R. Walk, A. White, D. Whyte, S. Wolfe, E. Wolfrum, Z. Yan, T. Zhang, A. U. the Alcator C-Mod, and D.-D. Teams, *Paper presented at the 25th IAEA Fusion Energy Conference Pribaltiyskaya, Russia* (2014), Paper no. EX/P6.
[7]A. E. White, P. Phillips, D. G. Whyte, A. E. Hubbard, C. Sung, J. W. Hughes, A. Dominguez, J. Terry, and I. Cziegler, Nucl. Fusion **51**, 113005 (2011).
[8]A. E. White, M. Barnes, A. Dominguez, M. Greenwald, N. T. Howard, A. E. Hubbard, J. W. Hughes, D. R. Mikkelsen, F. I. Parra, M. L. Reinke, C. Sung, J. Walk, and D. G. Whyte, Nucl. Fusion **54**, 083019 (2014).
[9]G. Bateman, A. H. Kritz, J. E. Kinsey, A. J. Redd, and J. Weiland, Phys. Plasmas **5**, 1793 (1998).
[10]M. Kotschenreuther, W. Dorland, M. A. Beer, and G. W. Hammett, Phys. Plasmas **2**, 2381 (1995).
[11]R. E. Waltz, G. M. Staebler, W. Dorland, G. W. Hammett, M. Kotschenreuther, and J. A. Konings, Phys. Plasmas **4**, 2482 (1997).
[12]J. Kinsey, G. M. Staebler, J. Candy, R. E. Waltz, and R. V. Budny, Nucl. Fusion **51**, 083001 (2011).
[13]V. Mukhovatov, Plasma Phys. Control. Fusion **45**, A235 (2003).
[14]X. Garbet, P. Mantica, F. Ryter, G. Cordey, F. Imbeaux, C. Sozzi, A. Manini, E. Asp, V. Parail, R. Wolf, and the JET EFDA Contributors, Plasma Phys. Control. Fusion **46**, 1351 (2004).
[15]X. Garbet, Y. Idomura, L. Villard, and T. H. Watanabe, Nucl. Fusion **50**, 043002 (2010).
[16]W. Horton, Rev. Mod. Phys. **71**, 735 (1999).
[17]G. T. Hoang, C. Bourdelle, X. Garbet, G. Giruzzi, T. Aniel, M. Ottaviani, W. Horton, P. Zhu, and R. Budny, Phys. Rev. Lett. **87**, 125001 (2001).
[18]D. R. Baker, C. M. Greenfield, K. H. Burrell, J. C. DeBoo, E. J. Doyle, R. J. Groebner, T. C. Luce, C. C. Petty, B. W. Stallard, D. M. Thomas, M. R. Wade, and D.-D. Team, Phys. Plasmas **8**, 4128 (2001).
[19]F. Ryter, C. Angioni, A. Peeters, F. Leuterer, H. U. Fahrbach, and W. Suttrop, Phys. Rev. Lett. **95**, 085001 (2005).
[20]Y. Camenen, A. Pochelon, A. Bottino, S. Coda, F. Ryter, O. Sauter, R. Behn, T. P. Goodman, M. A. Henderson, A. Karpushov, L. Porte, and G. Zhuang, Plasma Phys. Controlled Fusion **47**, 1971 (2005).
[21]P. Mantica, D. Strintzi, T. Tala, C. Giroud, T. Johnson, H. Leggate, E. Lerche, T. Loarer, A. G. Peeters, A. Salmi, S. Sharapov, D. V. Eester, P. C. de Vries, L. Zabeo, and K. D. Zastrow, Phys. Rev. Lett. **102**, 175002 (2009).
[22]J. C. Hillesheim, J. C. DeBoo, W. A. Peebles, T. A. Carter, G. Wang, T. L. Rhodes, L. Schmitz, G. R. McKee, Z. Yan, G. M. Staebler, K. H. Burrell, E. J. Doyle, C. Holland, C. C. Petty, S. P. Smith, A. E. White, and L. Zeng, Phys. Rev. Lett. **110**, 045003 (2013).
[23]J. Citrin, F. Jenko, P. Mantica, D. Told, C. Bourdelle, R. Dumont, J. Garcia, J. W. Haverkort, G. M. D. Hogeweij, T. Johnson, M. J. Pueschel, and J.-E. contributors, Nucl. Fusion **54**, 023008 (2014).
[24]M. Greenwald, R. L. Boivin, F. Bombarda, P. T. Bonoli, C. L. Fiore, D. Garnier, J. A. Goetz, S. N. Golovato, M. A. Graf, R. S. Granetz, S. Horne, A. Hubbard, I. H. Hutchinson, J. H. Irby, B. LaBombard, B. Lipschultz, E. S. Marmar, M. J. May, G. M. McCracken, P. O'Shea, J. E. Rice, J. Schachter, J. A. Snipes, P. C. Stek, Y. Takase, J. L. Terry, Y. Wang, R. Watterson, B. Welch, and S. M. Wolfe, Nucl. Fusion **37**, 793 (1997).
[25]T. K. Kurki-Suonio, K. H. Burrell, R. J. Groebner, R. Philipona, and C. L. Rettig, Nucl. Fusion **33**, 301 (1993).
[26]E. J. Doyle, W. A. Houlberg, Y. Kamada, V. Mukhovatov, T. H. Osborne, A. Polevoi, G. Bateman, J. W. Connor, J. G. Cordey, T. Fujita, X. Garbet, T. S. Hahm, L. D. Horton, A. E. Hubbard, F. Imbeaux, F. Jenko, J. E. Kinsey, Y. Kishimoto, J. Li, T. C. Luce, Y. Martin, M. Ossipenko, V. Parail, A. Peeters, T. L. Rhodes, J. E. Rice, C. M. Roach, V. Rozhansky, F. Ryter, G. Saibene, R. Sartori, A. C. C. Sips, J. A. Snipes, M. Sugihara, E. J. Synakowski, H. Takenaga, T. Takizuka, K. Thomsen, M. R. Wade, H. R. Wilson, I. T. P. T. Group, I. C. Database, M. T. Group, I. Pedestal, and E. T. Group, Nucl. Fusion **47**, S18 (2007).
[27]J. Candy and R. E. Waltz, J Comput. Phys. **186**, 545 (2003).
[28]N. T. Howard, A. E. White, M. Greenwald, M. L. Reinke, J. Walk, C. Holland, J. Candy, and T. Goerler, Phys. Plasmas **20**, 032510 (2013).
[29]N. T. Howard, C. Holland, A. E. White, M. Greenwald, and J. Candy, Phys. Plasmas **21**, 112510 (2014).
[30]J. W. Hughes, D. Mossessian, K. Zhurovich, M. DeMaria, K. Jensen, and A. E. Hubbard, Rev. Sci. Instrum. **74**, 1667 (2003).
[31]J. OShea, A. E. Hubbard, and A. C.-M. Group, in *Proceedings of 9th Joint Workshop on ECE and ECRH Borrego Springs* (1995), p. 7.
[32]A. Ince-Cushman, J. E. Rice, M. Bitter, M. L. Reinke, K. W. Hill, M. F. Gu, E. Eikenberry, C. Broennimann, S. Scott, Y. Podpaly, S. G. Lee, and E. S. Marmar, Rev. Sci. Instrum. **79**, 10E302 (2008).
[33]See http://w3.pppl.gov/transp, the official homepage of TRANSP for information concerning the models and methods employed in addition to usage documentation.
[34]C. C. Petty, T. C. Luce, J. C. DeBoo, R. E. Waltz, D. R. Baker, and M. R. Wade, Nucl. Fusion **38**, 1183 (1998).
[35]A. E. White, L. Schmitz, W. A. Peebles, T. L. Rhodes, T. A. Carter, G. R. McKee, M. W. Shafer, G. M. Staebler, K. H. Burrell, J. C. DeBoo, and R. Prater, Phys. Plasmas **17**, 020701 (2010).
[36]J. Candy and E. Belli, "The GYRO technical manual," https://github.com/gafusion/doc/raw/master/gyro/gyro_technical_manual.pdf.
[37]C. Holland, A. E. White, G. R. McKee, M. W. Shafer, J. Candy, R. E. Waltz, L. Schmitz, and G. R. Tynan, Phys. Plasmas **16**, 052301 (2009).
[38]N. T. Howard, A. E. White, M. L. Reinke, M. Greenwald, C. Holland, J. Candy, and J. R. Walk, Nucl. Fusion **53**, 123011 (2013).
[39]F. Jenko, W. Dorland, and G. W. Hammett, Phys. Plasmas **8**, 4096 (2001).
[40]M. Greenwald, A. Bader, S. Baek, M. Bakhtiari, H. Barnard, W. Beck, W. Bergerson, I. Bespamyatnov, P. Bonoli, D. Brower, D. Brunner, W. Burke, J. Candy, M. Churchill, I. Cziegler, A. Diallo, A. Dominguez, B. Duval, E. Edlund, P. Ennever, D. Ernst, I. Faust, C. Fiore, T. Fredian, O. Garcia, C. Gao, J. Goetz, T. Golfinopoulos, R. Granetz, O. Grulke, Z. Hartwig, S. Horne, N. Howard, A. Hubbard, J. Hughes, I. Hutchinson, J. Irby, V. Izzo, C. Kessel, B. LaBombard, C. Lau, C. Li, Y. Lin, B. Lipschultz, A. Loarte, E. Marmar, A. Mazurenko, G. McCracken, R. McDermott, O. Meneghini, D. Mikkelsen, D. Mossessian, R. Mumgaard, J. Myra, E. Nelson-Melby, R. Ochoukov, G. Olynyk, R. Parker, S. Pitcher, Y. Podpaly, M. Porkolab, M. Reinke, J. Rice, W. Rowan, A. Schmidt, S. Scott, S. Shiraiwa, J. Sierchio, N. Smick, J. A. Snipes, P. Snyder, B. Sorbom, J. Stillerman, C. Sung, Y. Takase, V. Tang, J. Terry, D. Terry, C. Theiler, A. Tronchin-James, N. Tsujii, R. Vieira, J. Walk, G. Wallace, A. White, D. Whyte, J. Wilson, S. Wolfe, G. Wright, J. Wright, S. Wukitch, and S. Zweben, Phys. Plasmas **21**, 110501 (2014).
[41]K. H. Burrell, Phys. Plasmas **4**, 1499 (1997).
[42]J. Rice, M. Reinke, C. Gao, N. Howard, M. Chilenski, L. Delgado-Aparicio, R. Granetz, M. Greenwald, A. Hubbard, J. Hughes, J. Irby, Y. Lin, E. Marmar, R. Mumgaard, S. Scott, J. Terry, J. Walk, A. White, D. Whyte, S. Wolfe, and S. Wukitch, Nucl. Fusion **55**, 033014 (2015).
[43]N. T. Howard, M. Greenwald, D. Mikkelsen, M. Reinke, A. White, D. Ernst, Y. Podpaly, and J. Candy, Nucl. Fusion **52**, 063002 (2012).
[44]C. Sung, "Experimental study of turbulent heat transport in Alcator C-Mod," Ph.D. dissertation, MIT, 2015.
[45]L. Lin, M. Pokerlab, E. M. Edmund, M. Greenwald, N. Tsujii, J. Candy, R. E. Waltz, and D. R. Mikkelsen, Plasma Phys. Controlled Fusion **51**, 065006 (2009).
[46]C. P. Kasten, A. E. White, and J. H. Irby, Phys. Plasmas **21**, 042305 (2014).
[47]A. J. Creely, E. M. Edlund, N. T. Howard, A. E. Hubbard, and A. E. White, in 56th Annual Meeting of the APS Division of Plasma Physics, 2014.
[48]C. Gao, J. Rice, H. Sun, M. Reinke, N. Howard, D. Mikkelson, A. Hubbard, M. Chilenski, J. Walk, J. Hughes, P. Ennever, M. Porkolab, A. White, C. Sung, L. Delgado-Aparicio, S. Baek, W. Rowan, M. Brookman, M. Greenwald, R. Granetz, S. Wolfe, E. Marmar, and T. A. C.-M. Team, Nucl. Fusion **54**, 083025 (2014).
[49]C. L. Fiore, D. R. Ernst, Y. A. Podpaly, D. Mikkelsen, N. T. Howard, J. Lee, M. L. Reinke, J. E. Rice, J. W. Hughes, Y. Ma, W. L. Rowan, and I. Bespamyatnov, Phys. Plasmas **19**, 056113 (2012).